Materials Science and Engineering A 371 (2004) 160–169

MATERIALS SCIENCE & ENGINEERING A

www.elsevier.com/locate/msea

Microstructures and mechanical properties of friction stir welds of 60% Cu–40% Zn copper alloy

Hwa Soon Park [a], Takahiro Kimura [b], Taichi Murakami [c,*], Yoshitaka Nagano [d], Kazuhiro Nakata [c], Masao Ushio [c]

[a] *Department of Materials Science and Engineering, Pukyong National University, San 100, Yongdang-Dong, Nam-Gu, Busan 608-739, South Korea*
[b] *Materials Science and Engineering Major, Graduate Student, Kansai University, 3-3-35 Yamate-cho, Suita, Osaka 564-8680, Japan*
[c] *Joining and Welding Research Institute, Osaka University, 11-1 Mihogaoka, Ibaraki, Osaka 567-0047, Japan*
[d] *Aluminum Technology Center, Showa Denko K.K., 1-480 Inuzuka, Oyama, Tochigi 323-8678, Japan*

Received 21 August 2003; received in revised form 14 November 2003

Abstract

The characteristics of the microstructures and mechanical properties of friction stir welds of 60% Cu–40% Zn alloy (60/40 brass) were investigated. The defect-free welds were obtained in a relatively wide range of welding conditions; the tool rotation speed ranged from 1000 to 1500 rpm with a welding speed from 500 to 2000 mm/min, and 500 rpm—500 mm/min. The microstructures of the welds yielded extremely fine grains with some deformed grains in the stirred zone (SZ) and elongated grains in the thermo-mechanically affected zone. The hardness values within the SZ in all welding conditions were much higher than those of the base metal, increased with a decrease in heat input. The generation of refined grains in the SZ was a main factor which caused the hardness increase associated with decreasing heat input. The strengths of the all-SZ showed relative correspondence to the variation of the hardness values in the SZ.

Keywords: Friction stir welding; 60% Cu–40% Zn copper alloy; 60/40 brass; Weldability; Microstructure; Mechanical property

1. Introduction

In many previous studies [1–7], it has mainly been demonstrated that friction stir welding (FSW) [8] produces low distortion, high-quality, low-cost welds of aluminum alloys, even for those difficult to conventional welding. The process can also be applied to copper and copper alloy [9–12], which are also known to cause difficulty in fusion welding, because it is essentially a solid state process without large distortion, solidification cracking, porosity, oxidation, and other defects that result from conventional fusion welding.

Although a few reports [9–12] have been made on the weldability of FSW for copper alloys, only a few attempts have been made thus far concerning the application of the FSW process for Cu–Zn alloys and observing in detail of the metallurgical and mechanical properties of the welds.

Thus, the objectives of this study are to clarify the appropriate welding conditions for sound welds, the behavior of defect formations, the detail of microstructures and mechanical properties, and the correspondence between the mechanical properties and microstructural changes in a wide range of the welding conditions for 60% Cu–40% Zn alloy.

2. Materials used and experimental procedures

Friction stir welds were produced in 60% Cu–40% Zn alloy (60/40 brass) plates of 2 mm thickness. The 60/40 brass used is a commercial JIS alloy No. C2801-1/4H. Tables 1 and 2 show the chemical composition and mechanical properties of this material, respectively.

To investigate the optimum conditions and microstructural characteristics associated with the formation of the stirred zone in a wide range of the welding conditions, bead-on-plate welds were made by a single pass of FSW. I-type butt welding was also carried out to evaluate the tensile properties of the FSW joints at a rotation speed of

* Corresponding author. Tel.: +81-6-6879-8666; fax: +81-6-6879-8689.
E-mail address: taichi@jwri.osaka-u.ac.jp (T. Murakami).

0921-5093/$ – see front matter © 2003 Elsevier B.V. All rights reserved.
doi:10.1016/j.msea.2003.11.030

Table 1
Chemical composition of the base metal used

Alloy	Chemical composition (mass%)								Remarks
	Cu	Pb	Fe	Sn	Zn	Al	Ni	P	
60/40 brass	60.89	0.003	0.003	–	39.10	–	–	–	C2801P-1/4H

Table 2
Mechanical properties of the base metal used

Alloy	Tensile properties			Hardness, HV
	Offset yield strength (MPa)	Ultimate tensile strength (MPa)	Elongation (%)	
60/40 brass	192	381	61	HV97

Table 3
Friction stir welding conditions for the bead-on-plate and the square groove butt welding

FSW conditions	Bead-on-plate welding	I groove butt welding
Dimension of specimen (mm)	50(W) × 100(l) × 2(t)	Two plates of 100(W) × 150(l) × 2(t)
Rotation speed (rpm)	250, 500, 1000 and 1500	1000
Welding speed (mm/min)	500, 1000, 1500 and 2000	500, 1000 and 2000

1000 rpm without defects in the bead-on-plate welds. The dimensions of the plates for bead-on-plate and square groove butt welding were 50(w) × 150 mm (l) and longitudinal two plates of 100(w) × 150 mm (l), respectively. The process parameters varied from 250 to 1500 rpm in counter clockwise tool rotation speed and from 500 to 2000 mm/min in welding speed. The welds were made on one side using two combinations of tool rotation speed and welding speed as shown in Table 3. The tilt angle for all welds was maintained at approximately 3°. The specimens were clamped tightly along the edges to a thick low carbon steel backup plate and to the table of the FSW facilities used to make the weld. The diameters of shoulder and probe of the tool used in this FSW were 12 and 4 mm, respectively. The length of the probe was 2 mm.

The generation of defects in the welds such as voids and lack of bonding were evaluated by visual and X-ray radiography inspections made on the welds.

The observations made of macro and microstructures were also done by an optical microscope and a scanning electron microscope (SEM) on a cross-section of the welds after polishing and etching with a solution of 100 ml distilled water, 15 ml hydrochloric acid, and 2.5 g iron(III) chloride. The sizes of grains in the α phase and the β phase and the ratio of their respective quantities in the welds were estimated by measuring the relative grain widths of both phases on all 15 lines drawn onto the five SEM images magnified by 5000× for each welding conditions.

The hardness measurements were taken along the centerline on the cross-section of the welds by using a Vickers hardness tester at a 0.49 N load.

The tensile properties of the FSW joints were evaluated on only the I-type butt welds at a tool rotation speed of 1000 rpm with welding speeds of 500, 1000 and 2000 mm/min. The tensile tests with two different configurations of specimens machined out from the as-welded plates were carried out at a cross head speed of 1.67×10^{-2} mm/s at room temperature. The principal axis of the transverse specimens with their as-welded joint surface conditions was perpendicular to the welding direction. The longitudinal specimens of the all stirred zone (all-SZ) had its principal axis parallel to the welding direction. The all-SZ specimens were made by machining 0.3 mm of the material from both the top and bottom surfaces as a means of skimming and eliminating some defects in the as-welded plates. The shape and dimensions of the joints and the all-SZ specimens are given in Fig. 1. The fractography of the tensile fracture surfaces was also discussed with a SEM.

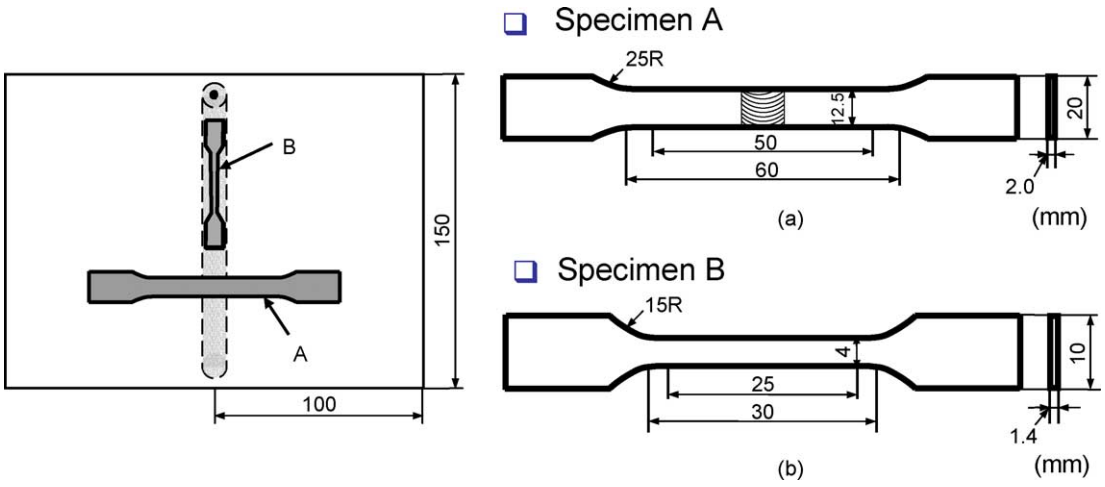

Fig. 1. Schematic of tensile test specimens for the joints (a) and the all-SZ (b).

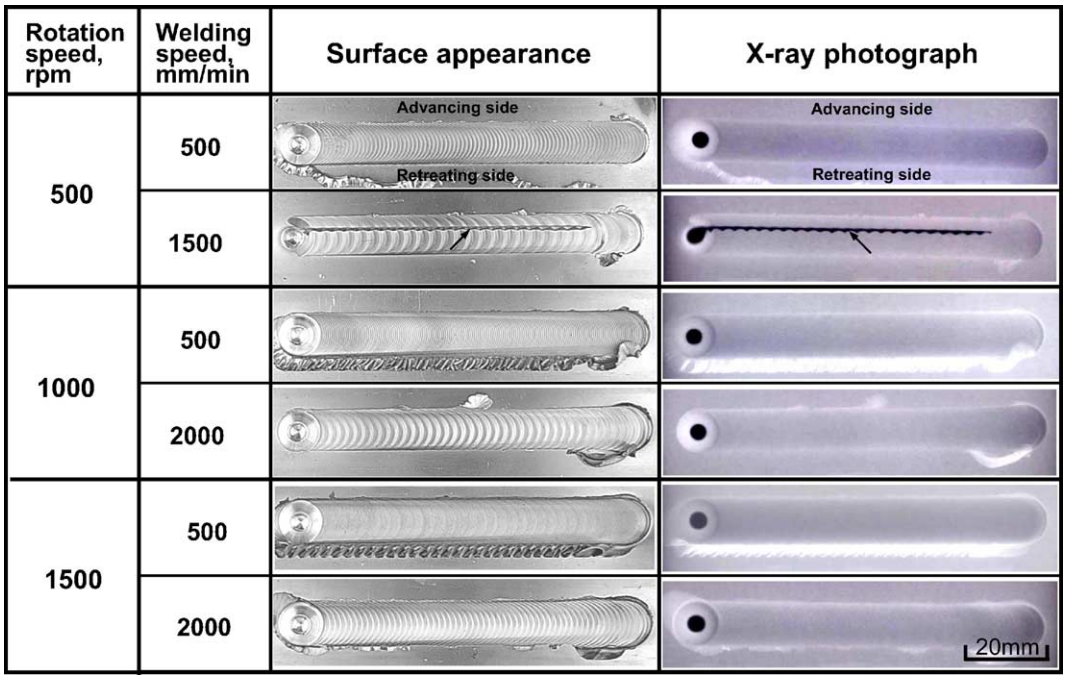

Fig. 2. Surface appearances and X-ray radiographs of the welds.

3. Results and discussion

3.1. Effect of FSW conditions on formation of welds

Fig. 2 displays the appearance of the bead surfaces and the X-ray radiographs of the bead-on-plate welds associated with the welding conditions. The defects of a groove-type void, which are indicated by arrows in the figure, were observed in the advancing side and lied linearly along the weld line at the welding conditions of low rotation speed 500 and 250 rpm. The frequency of generation of the defect increased with increasing welding speed at the rotation speed 500 rpm. The frequency of the defect also increased with a decrease in the rotation speed from 500 to 250 rpm.

From the visual and X-ray radiography inspections for the welds, the defect-free welds were obtained in all welding speeds of graduated rotation speed between 1000 and 1500 rpm, and 500 rpm—500 mm/min. This means that FSW for 60/40 brass is feasible in a relatively wide range of welding conditions. The FSW conditions resulting in sound welds are summarized in Fig. 3.

3.2. Characteristics of macro and microstructures in welds

Fig. 4 shows typical macrographs on a cross-section of the FSW welds associated with the welding conditions, where the wine cup features can be seen in the SZ at the welding conditions of sound welds. (The advancing side is on the right and the retreating side is on the left in all the figures of this study, unless otherwise noted.) The defects, which were caused by insufficient metal flow and low temperature rises, were almost observed as groove-type voids that almost reached bead surface in the advancing side near the boundary of SZ and thermo-mechanically affected zone (TMAZ) at low tool rotation speed 500 and 250 rpm. On the other hand, with the sound friction stirred welds, there were no defects on or inside the bead surface.

An example of a typical microstructure of the base metal, the TMAZ and the SZ is shown in Fig. 5. The base metal has a microstructure that consists of two phases, α (bright phase) and β (dark phase). The microstructures of 60/40

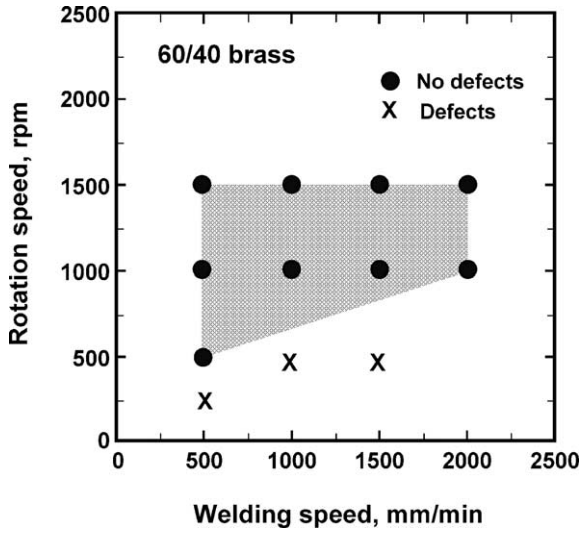

Fig. 3. Optimum welding conditions in the bead-on-plate welds.

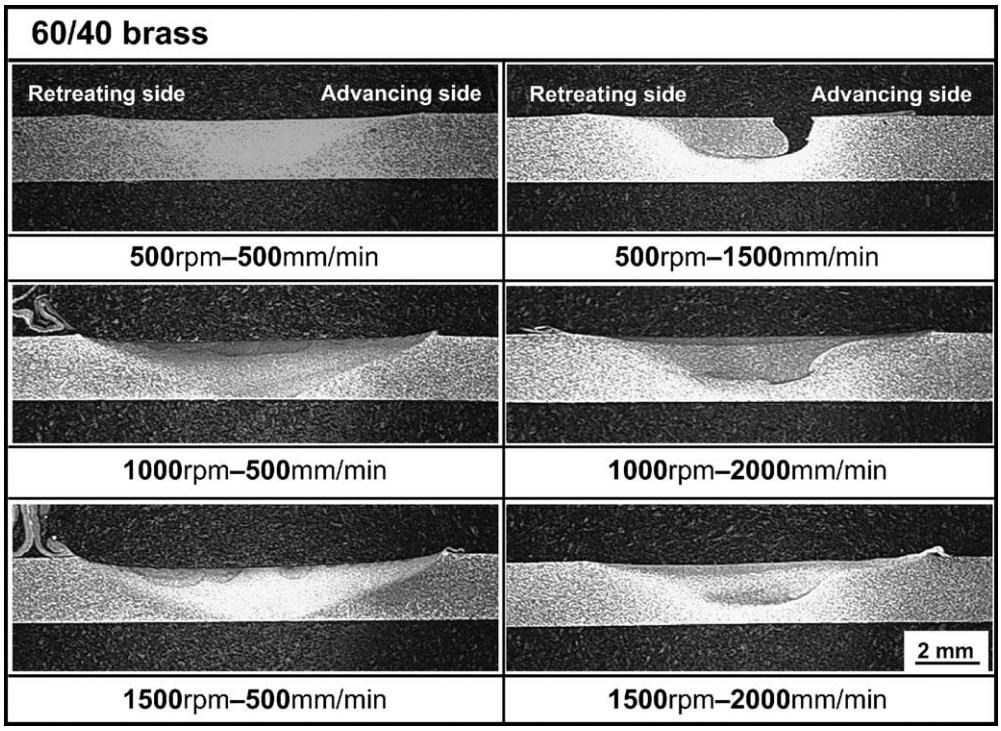

Fig. 4. Typical macrostructures in a cross-section of the welds associated with the welding conditions.

brass welds yielded extremely fine grains, in which there were portions with metal flow structures within the batch in the SZ generated by dynamic recrystallization due to frictional heat and deformation, and the elongated grains in the TMAZ. However, the HAZ was not clearly characterized in microstructures compared with the base metal.

The variation of microstructures in the SZ associated with the welding conditions is shown in Fig. 6. The grain sizes of α and β in the SZ in all the welding conditions are significantly smaller than that of the base metal. The range of the grain sizes of α in the SZ at the rotation speeds 1000 and 1500 rpm was estimated to be about 0.8–1.5 and 22.5 μm in

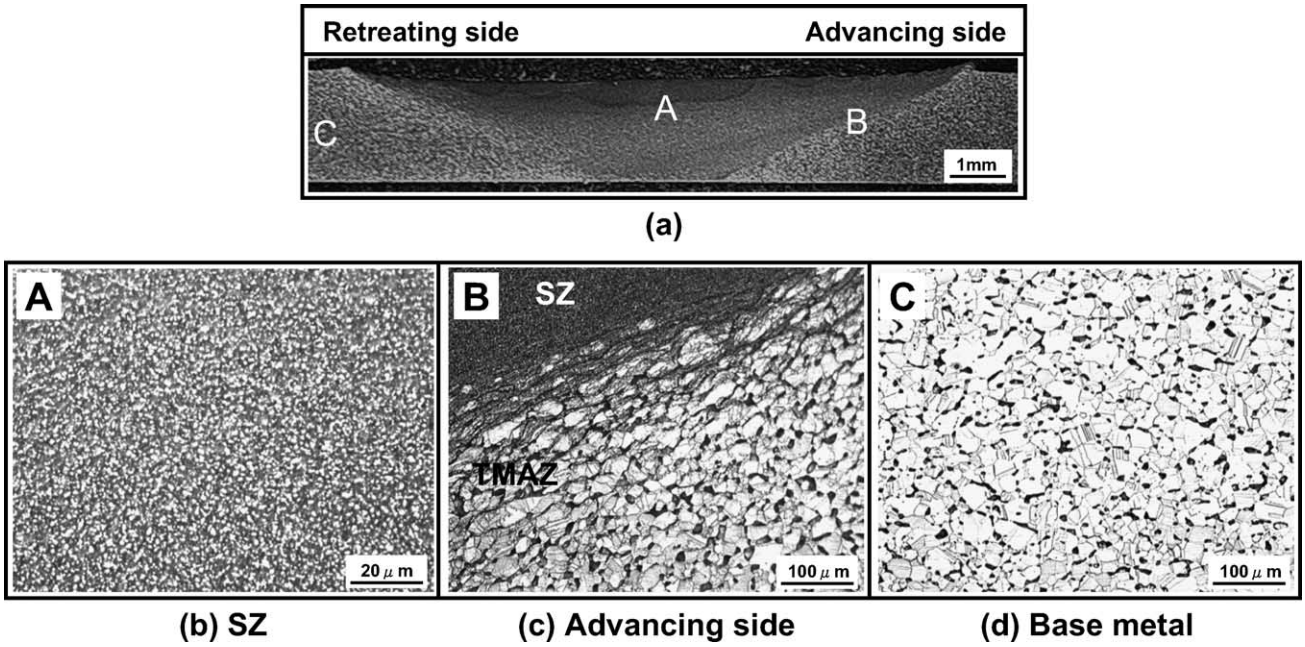

Fig. 5. Optical macro and microstructures in cross-section of the welds at 1000 rpm—500 mm/min.

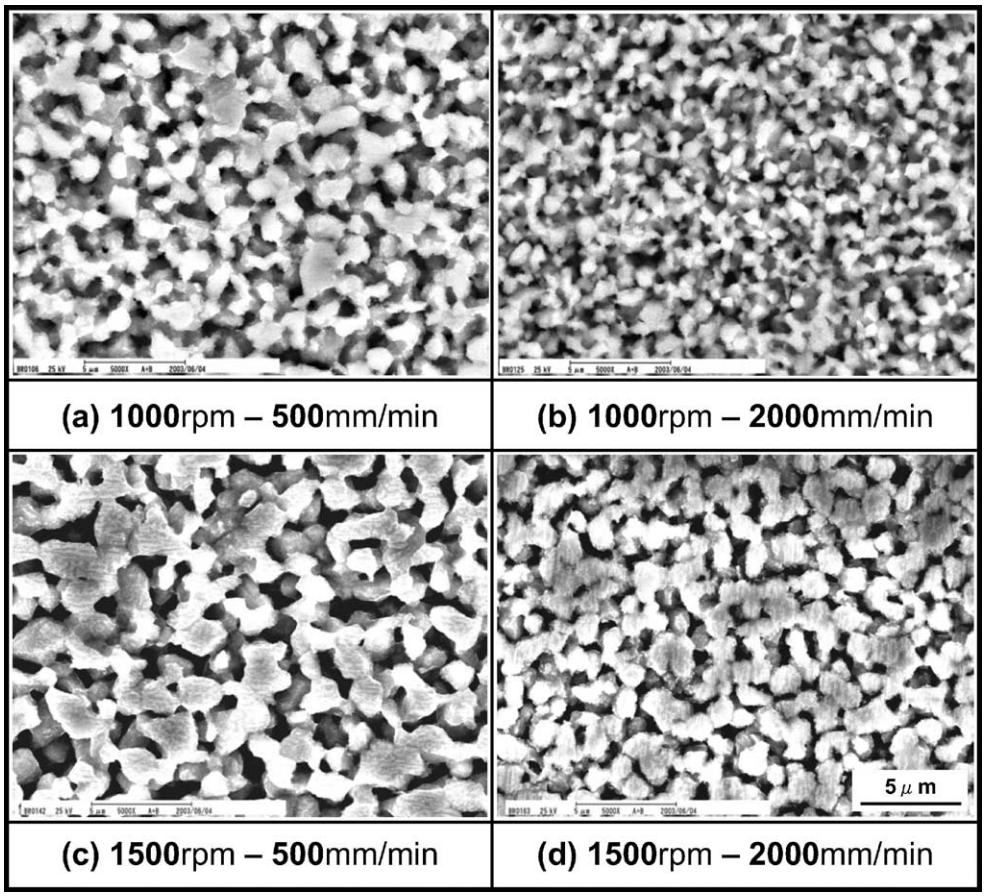

Fig. 6. Variation of SEM microstructures showing extremely fine grains in the SZ.

the base metal. The β grain sizes of 0.7–1.4 μm at the different welding conditions were also extremely small compared to that of 6.7 μm in the base metal. Moreover, the amount of β grains in the SZ, which was estimated to be 17–20%, was slightly larger than that, which was 16% in the base metal. However, the variation of the amount of β grains at various welding conditions was negligible. This suggests that the growth of recrystallized grains in the welds of 60/40 brass was not promoted rapidly during the weld thermal cycles. Furthermore, it was noted that the grains generated at higher welding speeds were smaller than those at lower welding speeds. For example, the grain sizes at the welding speeds of 500 and 2000 mm/min in the rotation speed 1000 rpm were about 1.0 and 0.8 μm, respectively. It was also confirmed that the grain sizes of both phases decreased with a decrease in rotation speed.

The total heat input Q generated by the FSW can be simply expressed through the following equation [13]:

$$Q = \left(\frac{4}{3}\right)\pi^2 \mu R_s P r^3$$

where μ is friction coefficient, R_s the tool rotation speed (rotations/s), P the vertical pressure (Pa) on the tool and r is surface radius (mm) of shoulder. According to the equation above, the FSW heat input Q is proportional to tool rotation speed R_s, so that the welding parameter R_s/W_s (W_s; welding speed, mm/min) represented in this study is closely related to welding heat input per unit length of the welded joints [14]. Fig. 7 shows the relationship between the welding parameter R_s/W_s and the grain size of α phase in the SZ at the rotation

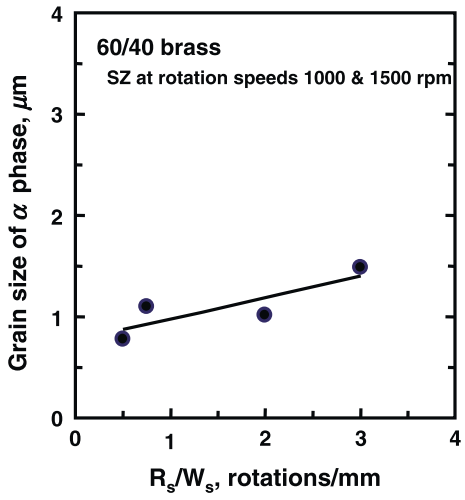

Fig. 7. Relationship between the welding parameter R_s/W_s and the grain size of α in the SZ at the rotation speeds 1000 and 1500 rpm.

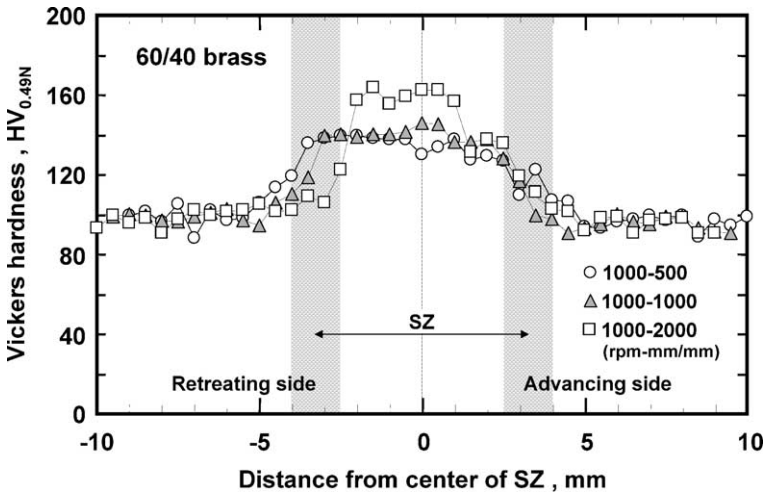

Fig. 8. Hardness profiles in cross-section of the welds at different welding speeds with the rotation speed 1000 rpm.

speeds 1000 and 1500 rpm. The grain size tends to decrease with decreasing R_s/W_s. Hence, it is concluded that the grain size in the SZ decreases with decreasing weld heat input.

3.3. Effect of welding conditions on mechanical properties

3.3.1. Hardness in welds

Fig. 8 shows the hardness profiles along the centerline on a cross-section of the welds at a tool rotation speed of 1000 rpm. The hardness values within the SZ including all the welding conditions are much higher than those of the base metal. The SZ at the welding speed 2000 mm/min has an average hardness of about HV160, which is about 1.7 times that of HV97 in the base metal. This is due to the generation of extremely fine grains in the SZ. The average hardness in the SZ at higher welding speed has higher values than that at lower welding speed. Any distinct differences in the hardness in the HAZ compared with that of the base metal remains unclear.

The variation of the maximum hardness values in the SZ is shown in Fig. 9. The hardness tends to increase with an increase in welding speed. It is considered that the variation of hardness is related to the microstructural changes in the SZ induced by welding conditions. As mentioned above, it is clear that the size of recrystallized grain varies with heat input. Therefore it is deducted that the generation of additionally refined grains in the SZ is a main factor that caused the hardness increase associated with decreasing heat input.

3.3.2. Tensile properties in welds

The tensile properties for the as-welded joints at the rotation speed 1000 rpm are shown in Fig. 10, which also includes the base metal properties. The joint at a welding speed of 500 mm/min fractured at the base metal region far from the weld center, and the tensile strength and 0.2% offset yield

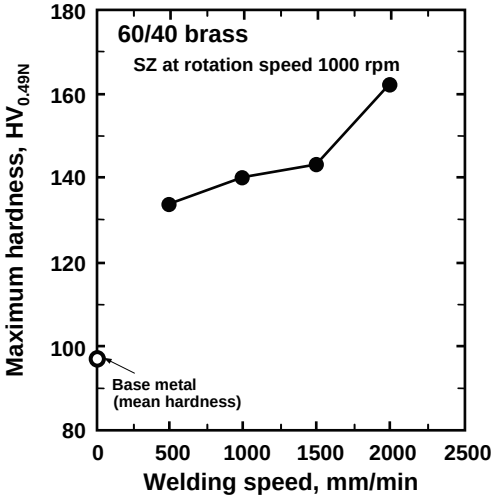

Fig. 9. Variation of maximum hardness in the SZ for welding speed at the rotation speed 1000 rpm.

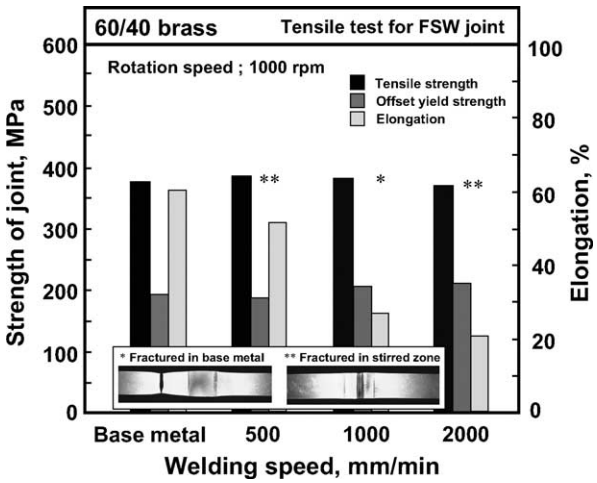

Fig. 10. Transverse tensile properties to welding direction of the joints at the different welding speeds with the rotation speed 1000 rpm.

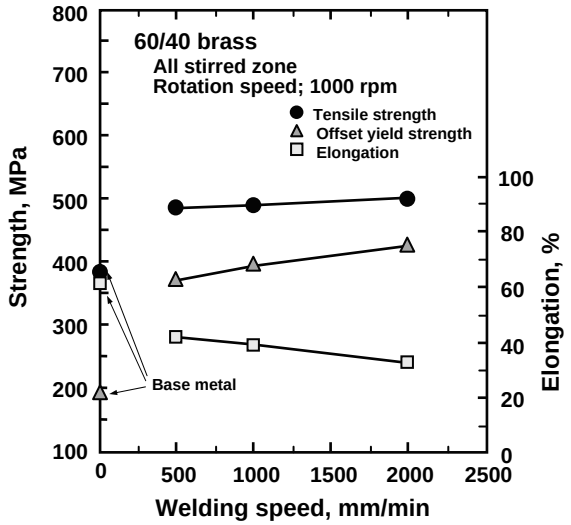

Fig. 11. Longitudinal tensile properties to welding direction of the all-SZ at the different welding speeds with the rotation speed 1000 rpm.

strength (offset yield strength) are almost the same as those of base metal. This means that the strength at the SZ and the TMAZ is higher than the base metal. This also matches well with the result of the hardness distribution of the welds as showed in Fig. 8. However, the joints at the welding speeds 1000 and 2000 mm/min were fractured near the center of the SZ and the strengths remained nearly unchanged as those of the joint at a welding speed of 500 mm/min.

The tensile properties for the longitudinal specimens of the all-SZ at the rotation speed 1000 rpm are shown in Fig. 11. The tensile strengths and offset yield strengths of the SZ including all the welding conditions are much higher than that of the base metal. On the other hand, the values of percent elongation are lower than that of the base metal, and tend to decrease with increasing welding speed. This suggests that the decrease of percent elongation is due to the increase of deformation resistance which resulted from the microstructural changes in the SZ as mentioned in 3.2 above. The strengths of the SZ increase with increasing welding speed, and the tendency is clearly revealed particularly in the offset yield strengths. Taking into general consideration the relationship between hardness and strength, the values and the variation of strengths of the SZ at various welding conditions correspond to those of hardness of the welds as mentioned in Section 3.3.1 above. Thus, it can also be stated that the strength increase in the SZ is caused by the variation of a great deal fine grains recrystallized by FSW.

As mentioned above, there are some differences in the results obtained by the tensile tests for the joints and the all-SZ at the rotation speed 1000 rpm. From the tensile tests for the joints, while the strengths of the all-SZ in all welding conditions were much higher than that of the base metal, the fractures occurred at the SZ at welding speeds of 1000 and

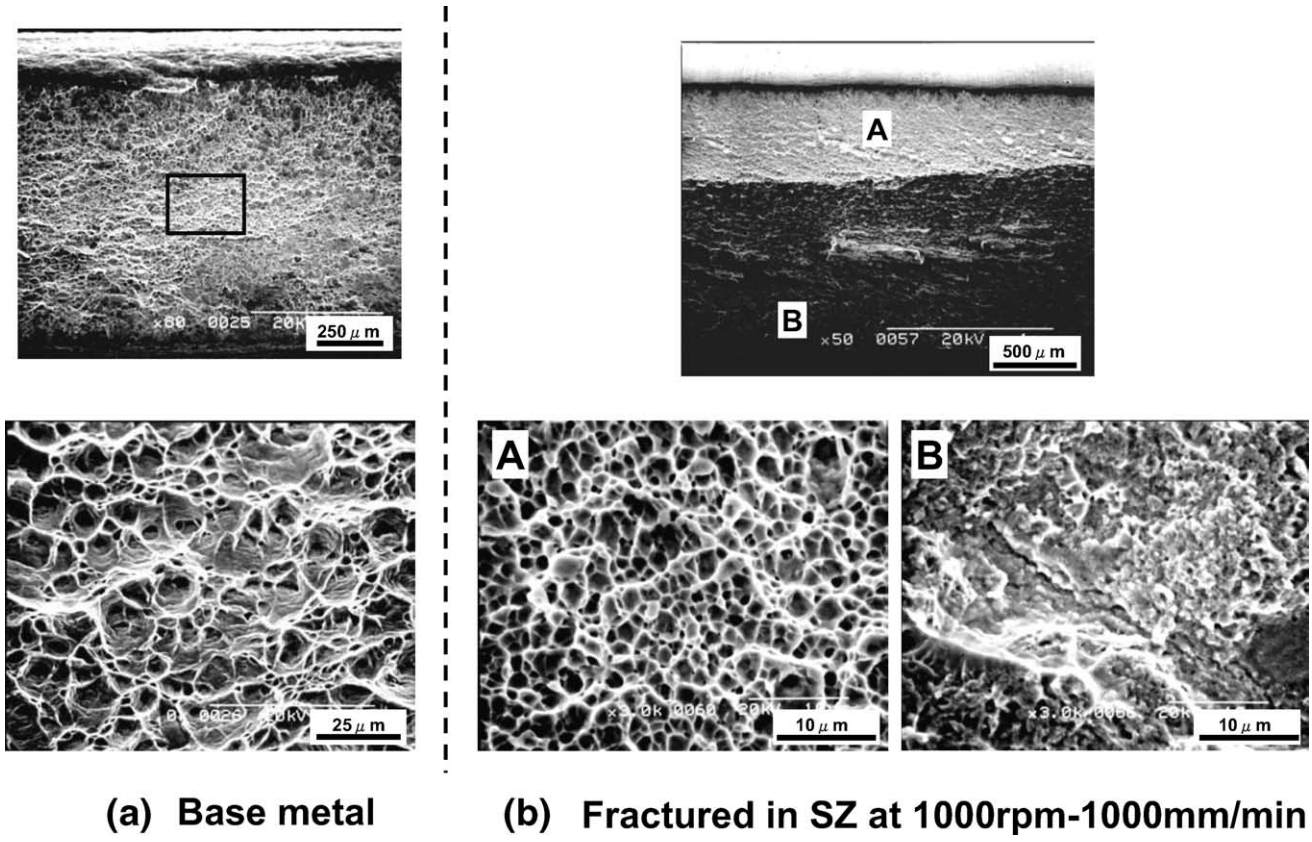

Fig. 12. SEM microfractographs of tensile fracture surfaces of the base metal (a) and the joints fractured in the SZ at 1000 rpm—1000 mm/min (b).

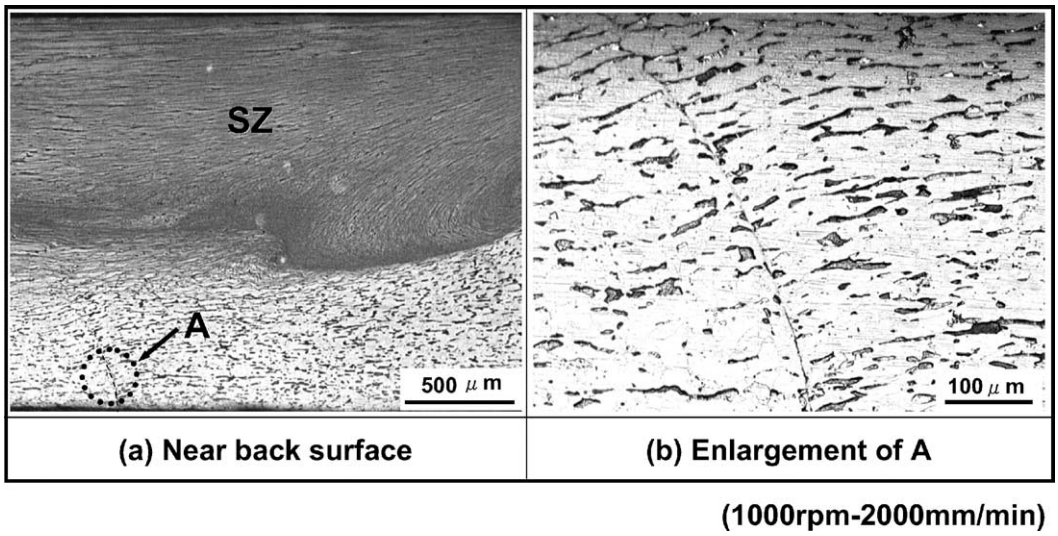

Fig. 13. Optical microstructures showing kissing bond near back surface of the welds at 1000 rpm—2000 mm/min, low and high magnifications of (a) and (b), respectively.

2000 mm/min. On the other hand, the joint fractured at the base metal region far from the weld center at welding speed 500 mm/min. The difference of the fracture location associated with the welding speed suggests that there are weak points such as defects or the region having lower strength of joining interface near the weld root side, which result in the initiation of tensile fracture.

In the observation of the fracture surface of the weld joints and the base metal, as shown in Fig. 12, that of the base metal shows a dimple pattern in the whole width of

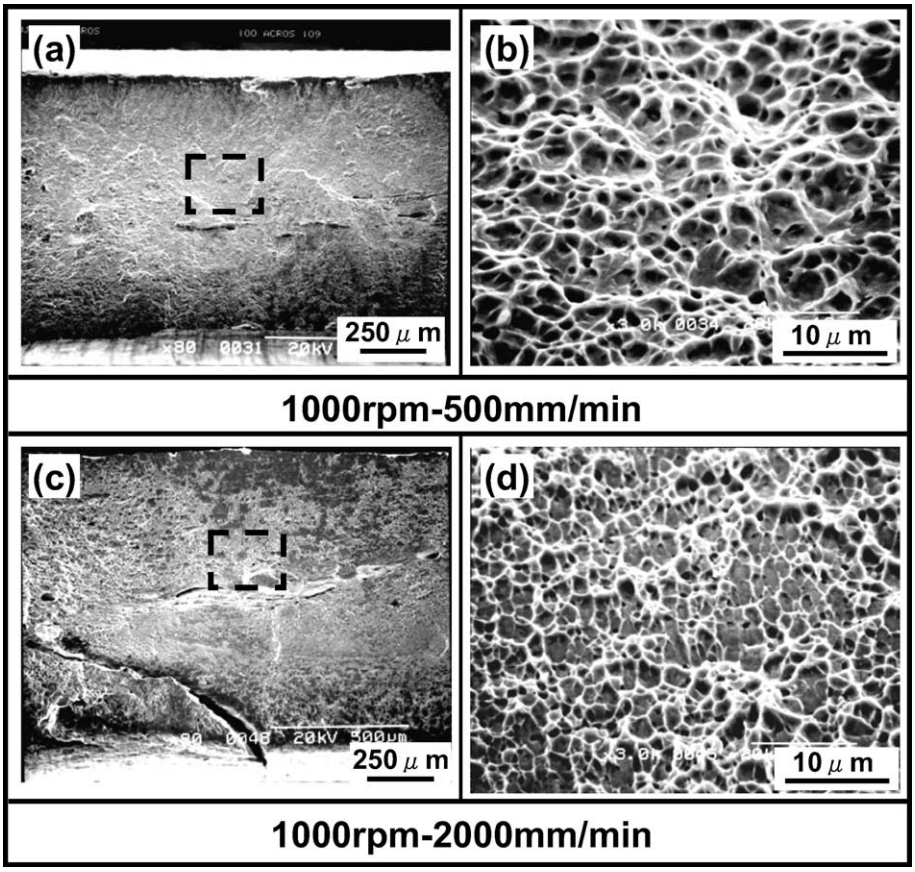

Fig. 14. SEM microfractographs of tensile fracture surfaces of the all-SZ at the different welding conditions with low magnification (a) and (c), and enlargement of each rectangle (b) and (d).

the specimen. The fracture surface of the specimens at a welding condition 1000 rpm—500 mm/min has nearly the same features as the base metal. However, in the specimens at the welding conditions 1000 rpm—1000 mm/min and 1000 rpm—2000 mm/min, fracture surface is approximately characterized with two regions of weld face side and weld root side. The weld face side shows a dimple pattern like that of the base metal, but the size of the dimples is much smaller than those of base metal. On the other hand, the weld root side consists of a flat and smooth surface with a small dimpled portion. Therefore, it is supposed that there are some flaws near the root side, which results in the initiation of tensile fracture.

The root flaw, namely kissing bond, is observed near the back surface of the welds at a welding speed of 2000 mm/min as shown in Fig. 13. Therefore, the fracturing in the SZ at the welding conditions is noted to be due to the existence of the kissing bond near the back surface. However, the tensile strength and offset yield strength are almost the same as those of the base metal. This means that the existence of the kissing bond has almost no influence on the strength of the joints at the welding conditions of this study.

In the observations of the tensile fracture surfaces of the all-SZ specimens, as shown in Fig. 14, it can be seen that the fracture surfaces have nearly the same feature of a dimple pattern like that of the base metal. However, the size of the dimples is much smaller than that of the base metal as showed in Fig. 12a. This means that the resistance for tensile deformation was enhanced by that the formation of the extremely fine grains at the SZ produced by FSW. The feature of the fracture surface also corresponds well with the strength increase of the SZ.

4. Conclusions

To clarify the feasibility of FSW process to 60/40 brass, the characteristics of structures, mechanical properties, and correspondence between mechanical properties and microstructural changes of friction stir welds were investigated in a wide range of the welding conditions. The main conclusions are summarized as follows:

(1) In a single pass of bead-on-plate welds, the defect-free welds that showed wine cup features were obtained in a relatively wide range of welding conditions, tool rotation speed of 1000–1500 rpm with the welding speed of 500–2000 mm/min, and 500 rpm—500 mm/min.
(2) The weld defect was formed as a groove-type void along the weld line at the advancing side at a low tool rotation speed of 250 rpm, and 500 rpm—1000 and 1500 mm/min.
(3) The microstructures of the welds at the rotation speeds 1000 and 1500 rpm showed extremely fine grains of 0.8–1.5 μm in mean diameter with some deformed grains in the SZ and elongated grains in the TMAZ. However, the HAZ was not clearly characterized in microstructures.
(4) The hardness values in the SZ were much higher, 1.4 to 1.7 times than those of the base metal, increased with decreasing heat input. The generation of additionally refined grains in the SZ was the main factor that caused the hardness increase associated with decreasing heat input.
(5) From the tensile tests for the joint, the joints at the welding speeds of 1000 and 2000 mm/min fractured near the center of SZ while the joints at a welding speed of 500 mm/min fractured at the base metal region far from the weld center. The kissing bond was observed near the back surface of the welds at a part of welding conditions. Therefore, the fracture that occurred at the SZ was affected by the existence of the kissing bond near back surface.
(6) From the tensile test for the all-SZ, the tensile strength and offset yield strength of the SZ including all the welding conditions were much higher than those of the base metal. The values of offset strengths showed more than about two times compared with that of the base metal. The strengths increased with decreasing heat input. The tendency was clearly revealed particularly in the offset yield strengths. The tensile properties showed a relative correspondence to the variation of the hardness values in SZ.

References

[1] C.J. Dawes, W.M. Thomas, Weld. J. 75 (1996) 41–45.
[2] C.G. Rhodes, M.W. Mahoney, W.H. Bingel, R.A. Spurling, C.C. Bampton, Scripta Materialia 36 (1997) 69–75.
[3] M.W. Mahoney, C.G. Rhodes, J.G. Flintoff, R.A. Spurling, W.H. Bingel, Metall. Mater. Trans. A 29A (1998) 1955–1964.
[4] L.E. Murr, G. Liu, J.C. McClure, J. Mater. Sci. 33 (1998) 1243–1251.
[5] O.V. Flores, C. Kennedy, L.E. Murr, D. Brown, S. Pappu, B.M. Nowak, J.C. McClure, Scripta Materialia 38 (1998) 703–708.
[6] T. Hashimoto, S. Jyogan, K. Nakata, Y.G. Kim, M. Ushio, in: Proceedings of the 1st International Symposium on Friction Stir Welding, Rockwell Science Center, Thousand Oaks, CA, USA, 14–16 June 1999.
[7] Y.S. Sato, M. Urata, H. Kokawa, Metall. Mater. Trans. A 33A (2002) 625–635.
[8] W.M. Thomas, E.D. Nicholas, J.C. Needham, M.G. Murch, P. Temple-Smith, C.J. Dawes, International Patent Application No. PCT/GB92/02203 and GB Patent Application No. 9125978.8, 6 December 1991.
[9] C.-G. Andersson, R.E. Andrews, in: Proceedings of the 1st International Symposium on Friction Stir Welding, Thousand Oaks, CA, USA, 14–16 June 1999.
[10] C.-G. Andersson, R.E. Andrews, B.G.I. Dance, M.J. Russel, E.J. Olden, R.M. Sanderson, in: Proceedings of the 2nd FSW Symposium on Comparison of Copper Canister Fabrication by the Electron Beam and Friction Stir Processes, Gothenburg, Sweden, 26–28 June 2000.

[11] K. Okamoto, M. Doi, S. Hirano, K. Aota, H. Okamura, Y. Aono, T.C. Ping, in: Proceedings of the 3rd International Symposium on Friction Stir Welding, Kobe, Japan, 27–28 September 2001.
[12] K.-S. Bang, W.-B. Lee, Y.-M. Yeon, S.-B. Jung, in: International Welding/Joining Conference-Korea 2002, Gyeongju, Korea, 28–30 October 2002, pp. 522–527.
[13] O. Frigaard, O. Grong, B. Bjorneklett, O.T. Midling, in: Proceedings of the 1st International Symposium on Friction Stir Welding, Thousand Oaks, CA, USA, 14–16 June 1999.
[14] K. Nakata, Y.G. Kim, M. Ushio, T. Hashimoto, S. Jyogan, ISIJ Int. 40 (2000) S15–S19.